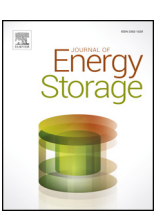
ELSEVIER

Contents lists available at ScienceDirect

Journal of Energy Storage

journal homepage: www.elsevier.com/locate/est



Integral capacitance of diffusion layer for rectangular structures



Wenxiao Zhou^a, Fuqian Yang^{b,*}

- ^a Department of Mechanical Engineering, University of Rochester, Rochester, NY 14604
- ^b Materials Program, Department of Chemical and materials Engineering, University of Kentucky, Lexington, KY 40506

ARTICLE INFO

Keywords: Electrical-double-layer capacitor Porous material Spectral method Integral capacitance

ABSTRACT

Electrical-double-layer capacitors are one of the important devices and systems used in energy storage. In the heart of the electrical-double-layer capacitors is the accumulation of ions/charges on the surfaces of "active" materials. Porous materials, such as carbon nanotubes and activated carbon, have been widely used in the electrical-double-layer capacitors due to large surface area. However, there are limited analytical solutions available for the calculation of the capacitance of porous materials. In this work, we use spectral method to solve linearized Poisson-Boltzmann equation under small electric potential for three different geometrical configurations and obtain analytical expressions of integral capacitances for slab-like structure, rectangular pore and 3D-rectangular box. The numerical results reveal that slit-like structures, such as multilayer graphene, are preferable for the energy storage in the electrical-double-layer capacitors. We also obtain analytical expressions of the integral capacitances for porous materials with parallel, cylindrical and rectangular-like pores of the same cross-sectional area, respectively. The results obtained in this work can also be applied to the design of electrodes of mesosizes and microsizes used in supercapacitors.

1. Introduction

The interest in increasing the use of renewable and "green" energies has stimulated the research to develop the technologies for energy storage. Electrochemical capacitors, which is also referred to as supercapacitors (SCs), have the potential as the devices and systems for energy storage due to the unique characteristics of high power density, fast charge/discharge rate, and long cycling life [1,2]. Electrochemical capacitors can be divided into groups: one is electric double-layer capacitors (EDLCs), which is based on accumulation of electrolyte ions on the surface of "active" materials, such as carbon, without charge transfer [3-5]; the other is pseudo-capacitors, which involves the transfer of electron between electrode and electrolyte, redox reactions and intercalation processes. EDLCs generally exhibit better long-term cycling stability and rate performance than pseudo-capacitors [6,7].

The principle of the storage of ions/charge in EDLCs is similar to parallel capacitors, and the capacitance of EDLCs can be calculated from two capacitors of a compact layer (Helmholtz layer) and a diffuse layer in a series connection. The capacitance of the diffuse layer for a symmetric-binary electrolyte can be calculated from the Poisson-Boltzmann equation [4,8] as

$$\nabla^2 \Phi = \frac{2zeC_0}{\epsilon_0 \epsilon_r} \sinh\left(\frac{ze\Phi}{kT}\right) \text{for } \mathbf{r} \in V$$
(1)

 $\ensuremath{^{\circ}}$ Corresponding author.

E-mail address: fyang2@uky.edu (F. Yang).

and the corresponding boundary conditions. Here, Φ is electric potential inside the diffuse layer, \in $_0$ is the dielectric constant of vacuum, \in $_r$ is the relative dielectric constant of electrolyte, z is the valence of ions, e is the electronic charge, C_0 is the concentration of electrolyte ions, k is the Boltzmann constant, T is absolute temperature, V is the domain of the diffusion layer, and \mathbf{r} represents spatial position. Equation (1) takes account of random thermal motion of ions, electrostatic interaction and spatial distribution of ions, while ions are approximated as point charges and no short-range interactions, such as ion-solvent and ion-ion, are considered [9,10]. The spatial distribution of ions at equilibrium is calculated from the electric potential inside the diffuse layer as

$$C^{\pm} = C_0^{\pm} \sinh\left(-\frac{ze\Phi}{kT}\right) \tag{2}$$

with the superscripts of +/- representing positive/negative ions. Note that various modifications of Eq. (1) have been proposed to include the contributions of ionic sizes and the interaction between ions [11,12], such as Bikerman's model [13], which generally introduce a modified parameter, including the contribution of ionic size/steric factor, in Eq. (1). Recently, one-dimensional Ising model has been used to analyze electrical double layers of a flat electrode [14] and a nanopore [15]. However, the use of the Ising model in the analyses of two- and three-

dimensional structures requires numerical calculation due to nonlinear characteristic of the Ising model.

For small electric potential with $|ze\Phi/kT| < 1$, the first order approximation of the term $\sinh(ze\Phi/kT)$ is equal to $ze\Phi/kT$, and linearized Poisson-Boltzmann equation is obtained as

$$\nabla^2 \Phi = \frac{2zeC_0}{\epsilon_0 \epsilon_r} \left(\frac{ze\Phi}{kT} \right) \tag{3}$$

Currently, closed-form solutions of Eq. (1) are limited to slab-like electrodes due to the nonlinear characteristic of hyperbolic sine. Two approaches have been used to calculate the capacitance in the diffuse layer for EDLCs; the first one uses either the linearized Poisson-Boltzmann equation of (3) for small electric potential or approximation methods for specific geometrical shapes [16-20], including cylindrical shape (cylinder and cylindrical pore) and spherical shape (sphere and spherical cavity), and the other uses numerical methods to solve the nonlinear equation of (1) and calculate the capacitance of a given electrode [21-23]. However, there is no closed-form solution available for rectangular electrodes in literature even for the linearized Poisson-Boltzmann equation of (3). Note that numerical methods have been extensively used to solve the modified Poisson-Boltzmann equations due to the nonlinear characteristics.

It is known that active carbons are porous and have been extensively used in EDLCs. There is a wide range of topologies for the porous structures of active carbons, including cylindrical pores and layer structures, and most pore structures in active carbons are irregular. It would be of practical importance to determine the effect of the pore structure on the storage of ions/charge, i.e. the dependence of the capacitance of the diffusion layer on the pore structure. In this work, we consider three different structures of slab-like structure, rectangular pore, and 3D rectangular box. Under the condition of small electric potential, we use spectral method [24] to solve the linearized Poisson-Boltzmann equation of (3) and calculate the capacitance of the diffuse layer for all the three different geometrical structures. The dependence of the integral capacitance on the aspect ratio of the rectangular pore and 3D rectangular box is analyzed. Comparisons of the integral capacitances are made between the rectangular pore and a cylindrical pore of the same cross-section area and between the 3D rectangular box and a spherical cavity of the same volume. It needs to be pointed out that the results presented in this work cannot be applied to the structures with characteristic dimension comparable to the size of electrolyte ions, such as nanopores. For structures with characteristic dimension comparable to the size of electrolyte ions, one needs to use the modified Poisson-Boltzmann equations, which take into account the contribution of ionic size, and numerical method in the analysis of the structural dependence of capacitance.

2. Mathematical Formulation

The Debye-Hückel constant, $\kappa,$ as a function of the concentration of electrolyte ions is

$$\kappa = \left(\frac{2z^2 e^2 C_0}{\epsilon_0 \epsilon_r kT}\right)^{1/2} \tag{4}$$

Substituting Eq. (4) in Eq. (3) yields

$$\nabla^2 \Phi = \kappa^2 \Phi \tag{5}$$

The boundary condition for the linearized Poisson-Boltzmann equation is

$$\Phi = \Phi_0 \text{ for } \mathbf{r} \in \partial V \tag{6}$$

where Φ_0 is the electric potential at the boundary of the diffuse layer, ∂V . Introducing auxiliary variable, Ψ , as $\Psi = (\Phi - \Phi_0)/\Phi_0$, we have

$$\nabla^2 \Psi = \kappa^2 \Psi + \kappa^2 \tag{7}$$

and

$$\Psi = 0 \text{ for } \mathbf{r} \in \partial V \tag{8}$$

The charge density at the boundary of the diffuse layer is calculated as

$$\rho|_{\partial V} = -\epsilon_0 \in_r \left. \frac{d\Phi}{dn} \right|_{\partial V} = -\epsilon_0 \in_r \Phi_0 \frac{d\Psi}{dn} \right|_{\partial V} \tag{9}$$

from which the total charge stored in the diffusion layer, Q, is calculated as

$$Q = \int_{\partial V} \rho dS \tag{10}$$

Using Eq. (10), the integral capacitance of the diffusion layer per unit area is found as

$$C_{IL} = \frac{Q}{A\Phi_0} = -\frac{\epsilon_0 \epsilon_r}{A} \int_{\partial V} \frac{d\Psi}{dn} \bigg|_{\partial V} dS$$
 (11)

where *A* is the total surface area of the diffusion layer. According to Eq. (11), the integral capacitance of the diffusion layer for small electric potential is independent of the applied electric potential and depends only on the geometrical structure of the diffusion layer. Note that the proportionality between the total charge stored in the diffusion layer and the electric potential indicates that the integral capacitance of the diffusion layer is the same as the differential capacitance of the diffusion layer for small electric potential.

3. Capacitance of diffusion layer of three different geometries

In the following analyses, we focus on three different geometries of slab-like structure, rectangular pore and 3D rectangular box, as shown in Fig. 1.

3.1. Slab-like structure

For a slab-like structure of 2a in the separation, the slab structure is similar to a parallel capacitor. For the symmetric charging of the slab structure, the electric potentials of both plates are same. The boundary

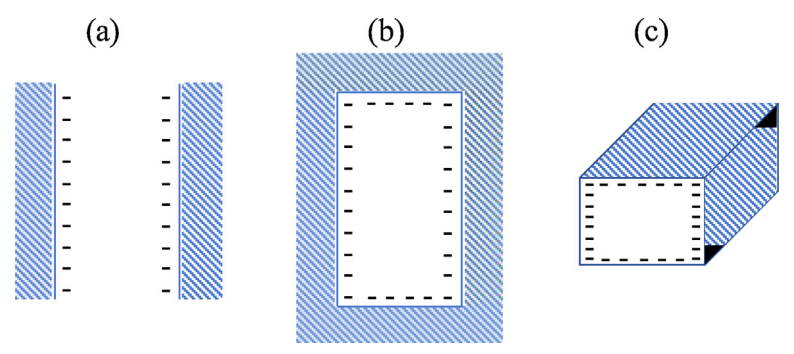


Figure 1. Schematic of geometric configurations of electrochemical double layer: (a) slab-like structure, (b) rectangular pore, and (c) 3D rectangular box

conditions are $\Psi|_{x=a}=0$ and $(d\Psi/dx)|_{x=0}=0$. Using the spectral method, we note that the eigenfunctions and eigenvalues of the equation, $d^2\Psi/dx^2=0$ are

$$\psi_n = \cos\left(n + \frac{1}{2}\right) \frac{\pi x}{a} \text{ and } \lambda_n^2 = \left(n + \frac{1}{2}\right)^2 \frac{\pi^2}{a^2} n = 0, 1, 2, \dots$$
 (12)

Expanding Ψ and κ^2 in the eigenfuctions as

$$\Psi(x) = \sum_{n=0}^{\infty} u_n \psi_n(x) \text{ and } \kappa^2 = \sum_{n=0}^{\infty} f_n \psi_n(x)$$
(13)

we have

$$\sum_{n=0}^{\infty} (\lambda_n^2 + \kappa^2) u_n \psi_n(x) = -\sum_{n=0}^{\infty} f_n \psi_n(x)$$
 (14)

The solutions of u_n are

$$u_n = -\frac{f_n}{(\kappa^2 + \lambda_n^2)} \tag{15}$$

which gives the solution of the auxiliary function, Ψ , as

$$\Psi(x) = -\sum_{n=0}^{\infty} \frac{f_n}{(\kappa^2 + \lambda_n^2)} \cos\left(n + \frac{1}{2}\right) \frac{\pi x}{a}$$
(16)

Here, the coefficients, f_n , are

$$f_n = \frac{4(-1)^n \kappa^2}{(2n+1)\pi} \tag{17}$$

Substituting Eq. (16) into Eq. (11) yields the integral capacitance per unit area as

$$C_{IL} = 8 \in_{0} \in_{r} a\kappa^{2} \sum_{n=0}^{\infty} \frac{1}{4a^{2}\kappa^{2} + (2n+1)^{2}\pi^{2}}$$
(18)

3.2. Rectangular pore

For a rectangular pore of 2a in length and 2b in width, the boundary conditions for Eq. (7) are

$$\Psi|_{x=a} = \Psi|_{x=b} = 0 \text{ and } (d\Psi/dx)|_{x=0} = (d\Psi/dy)|_{y=0} = 0$$
 (19)

The eigenfunctions for two-dimensional Laplace equation with the boundary conditions of (19) are

$$\psi_{nm}(x, y) = \cos\left(n + \frac{1}{2}\right) \frac{\pi x}{a} \cos\left(m + \frac{1}{2}\right) \frac{\pi y}{b} (n, m = 0, 1, 2, ...)$$
 (20)

with eigenvalues as

$$\lambda_{nm}^2 = \left(n + \frac{1}{2}\right)^2 \frac{\pi^2}{a^2} + \left(m + \frac{1}{2}\right)^2 \frac{\pi^2}{b^2} \tag{21}$$

Following the approach used in the analysis of the electric potential of the slab-like structure, we express the auxiliary function, Ψ , and κ as

$$\Psi(x, y) = \sum_{n,m=0}^{\infty} u_{nm} \psi_{nm}(x, y) \text{ and } \kappa^2 = \sum_{n,m=0}^{\infty} f_{nm} \psi_{nm}(x, y)$$
 (22)

Substituting Eq. (22) in Eq. (7) yields

$$\sum_{n,m=0}^{\infty} (\lambda_{nm}^2 + \kappa^2) u_{nm} \psi_{nm}(x, y) = -\sum_{n,m=0}^{\infty} f_{nm} \psi_{nm}(x, y)$$
(23)

The solutions of u_{nm} are

$$u_{nm} = -\frac{f_{nm}}{(\kappa^2 + \lambda_{nm}^2)} \tag{24}$$

which gives the solution of the auxiliary function, Ψ , as

$$\Psi(x,y) = -\sum_{n,m=0}^{\infty} \frac{f_{nm}}{(\kappa^2 + \lambda_{nm}^2)} \cos\left(n + \frac{1}{2}\right) \frac{\pi x}{a} \cos\left(m + \frac{1}{2}\right) \frac{\pi y}{b}$$
(25)

Here, the coefficients, f_{nm} , are

$$f_{nm} = \frac{16(-1)^{n+m}\kappa^2}{(2n+1)(2m+1)\pi^2}$$
(26)

Substituting Eq. (25) into Eq. (11) yields the integral capacitance per unit area as

$$C_{IL} = \frac{16ab \in_{0} \in_{r} \kappa^{2}}{(a+b)\pi^{2}} \sum_{n,m=0}^{\infty} \frac{1}{(\kappa^{2} + \lambda_{nm}^{2})} \left(\frac{1}{(2m+1)^{2}a^{2}} + \frac{1}{(2n+1)^{2}b^{2}} \right)$$
(27)

For the limiting case, $b{\to}\infty$, we have $\lambda_{nm}{\to}\lambda_n$. Equation (27) is simplified to as

$$C_{IL} = \frac{16 \in_{0} \in_{r} \kappa^{2}}{a\pi^{2}} \sum_{n,m=0}^{\infty} \frac{1}{(2m+1)^{2}(\kappa^{2} + \lambda_{n}^{2})}$$

$$= \frac{2 \in_{0} \in_{r} \kappa^{2}}{a} \sum_{n,m=0}^{\infty} \frac{1}{(\kappa^{2} + \lambda_{n}^{2})}$$
(28)

which is the same as Eq. (18). Note that the following equality is used in obtaining Eq. (28).

$$\sum_{n=0}^{\infty} \frac{1}{(2n+1)^2} = \frac{\pi^2}{8} \tag{29}$$

3.3. 3D Rectangular box

For a 3D rectangular box of 2a in length, 2b in width and 2c in depth, the boundary conditions for Eq. (7) are

$$\Psi|_{x=a} = \Psi|_{x=b} = \Psi|_{x=c} = 0 \text{ and } (d\Psi/dx)|_{x=0}$$

$$= (d\Psi/dy)|_{y=0} = (d\Psi/dz)|_{z=0} = 0$$
(30)

The eigenfunctions for three-dimensional Laplace equation with the boundary conditions of (30) are

$$\psi_{nm}(x, y, z) = \cos\left(n + \frac{1}{2}\right) \frac{\pi x}{a} \cos\left(m + \frac{1}{2}\right) \frac{\pi y}{b} \cos\left(p + \frac{1}{2}\right) \frac{\pi z}{c}$$

$$(n, m, p = 0, 1, 2, ...)$$
(31)

with eigenvalues as

$$\lambda_{nmp}^2 = \left(n + \frac{1}{2}\right)^2 \frac{\pi^2}{a^2} + \left(m + \frac{1}{2}\right)^2 \frac{\pi^2}{b^2} + \left(p + \frac{1}{2}\right)^2 \frac{\pi^2}{c^2}$$
(32)

Following the approach used in the analysis of the electric potential of the rectangular pore, we express the auxiliary function, Ψ , and κ as

$$\Psi(x, y, z) = \sum_{n,m,p=0}^{\infty} u_{nmp} \psi_{nmp}(x, y, z) \text{ and } \kappa^2 = \sum_{n,m,p=0}^{\infty} f_{nmp} \psi_{nmp}(x, y, z)$$
(33)

Substituting Eq. (33) in Eq. (7) yields

$$\sum_{n,m,p=0}^{\infty} (\lambda_{nmp}^2 + \kappa^2) u_{nmp} \psi_{nmp}(x, y, z) = -\sum_{n,m,p=0}^{\infty} f_{nmp} \psi_{nmp}(x, y, z)$$
(34)

The solutions of u_{nmp} are

$$u_{nmp} = -\frac{f_{nmp}}{(\kappa^2 + \lambda_{nmp}^2)} \tag{35}$$

which gives the solution of the auxiliary function, Ψ , as

$$P(x, y, z) = -\sum_{n,m,p=0}^{\infty} \frac{f_{nmp}}{(\kappa^2 + \lambda_{nmp}^2)} \cos\left(n + \frac{1}{2}\right) \frac{\pi x}{a} \cos\left(m + \frac{1}{2}\right) \frac{\pi y}{b} \cos\left(p + \frac{1}{2}\right) \frac{\pi z}{c}$$
(36)

Here, the coefficients, f_{nmp} , are

$$f_{nmp} = \frac{64(-1)^{n+m+p}\kappa^2}{(2n+1)(2m+1)(2p+1)\pi^3}$$
(37)

Substituting Eq. (36) into Eq. (11) yields the integral capacitance per unit area as

$$C_{IL} = \frac{128abc \in_{0} \in_{r} \kappa^{2}}{\pi^{4}(ab + bc + ac)} \sum_{n,m,p=0}^{\infty} \frac{1}{(\kappa^{2} + \lambda_{nmp}^{2})(2n + 1)^{2}(2m + 1)^{2}(2p + 1)^{2}}$$
(38)

$$\left(\frac{(2n+1)^2}{a^2} + \frac{(2m+1)^2}{b^2} + \frac{(2p+1)^2}{c^2}\right)$$

For $c \rightarrow \infty$, there is $\lambda_{nmp} \rightarrow \lambda_{nm}$. Equation (38) reduces to

$$\frac{C_{IL}}{e^{2}} = \frac{16 \in_{0} \in_{r} \kappa^{2}}{(a+b)\pi^{2}} \sum_{n,m=0}^{\infty} \frac{1}{(2n+1)(2m+1)(\kappa^{2}+\lambda_{nm}^{2})} \left(\frac{2m+1}{2n+1}\frac{a}{b} + \frac{2n+1}{2m+1}\frac{b}{a}\right)$$
(39)

which is the same as Eq. (27). Note that Eq. (29) is used to simplify Eq. (38) to Eq. (39) for $c \rightarrow \infty$.

4. Numerical calculation

As pointed out in the introduction, the only closed-form solution of the nonlinear Poisson-Boltzmann equation of (1) available in literature is for the slab-like structure, and the closed-form solutions of the linearized Poisson-Boltzmann equation of (3) available in literature are for the slab-like structure, cylindrical shape (cylinder and cylindrical pore) and spherical shape (sphere and spherical cavity). Here, we limit the following discussion to the linearized Poisson-Boltzmann equation of (3).

For the slab-like structure with small electric potential and symmetric charging, i.e. $\Phi|_{x=a} = \Phi_0$ and $(d\Phi/dx)|_{x=0} = 0$, the solution of Eq. (3) can be easily found as

$$\Phi = \Phi_0 \frac{\cosh \kappa \alpha}{\cosh \kappa a} \tag{40}$$

which gives the integral capacitance per unit area as

$$C_{IL} = \frac{\sigma}{\Phi_0} = \epsilon_r \epsilon_0 \kappa \tanh \kappa a \tag{41}$$

Figure 2 shows the variation of the integral capacitance per unit area of the slab-like structure with the parameter of κa . For the purpose of comparison, both the results of Eq. (18) and are depicted in Fig. 2. It

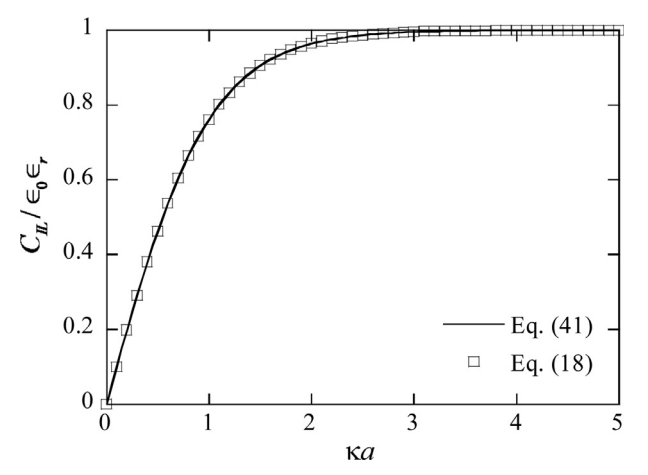


Figure 2. Variation of integral capacitance per unit area with κa for slab-like structure (The solid line represents the analytical solution, and the square symbols represent the spectral solution.)

is evident that the spectral solution of (18) is in good accord with the analytical solution of (41). For large value of κa , the interaction between two plates is negligible, and the integral capacitance per unit area approaches $\in {}_0 \in \mathcal{K}$ for a single plate. The spectral method provides an approach to obtain the solutions of the linearized Poisson-Boltzmann equation and the analytical expressions of the integral capacitance of some geometrical structures.

Consider a straight pore of A in cross-sectional area. For a cylindrical pore, the radius of the cylindrical pore with A in cross-sectional area is $(A/\pi)^{1/2}$, and the integral capacitance per unit area for small electric potential is

$$C_{IL} = \in_r \in_0 \kappa \cdot \frac{I_1(\kappa \sqrt{A/\pi})}{I_0(\kappa \sqrt{A/\pi})}$$
(42)

where $I_0(\cdot)$ and $I_1(\cdot)$ are the modified Bessel functions of the first kind of the zeroth and first order, respectively. Using Eq. (42), we obtain the integral capacitance per unit length of the cylindrical pore as

$$C_{I} = 2\pi r C_{IL} = 2 \in_{r} \in_{0} \kappa \sqrt{A\pi} \cdot \frac{I_{1}(\kappa \sqrt{A/\pi})}{I_{0}(\kappa \sqrt{A/\pi})}$$

$$\tag{43}$$

For a rectangular pore of A in cross-sectional area, a = A/4b, Eq. (27) becomes

$$C_{IL} = \frac{32 \in_{0} \in_{r} \sqrt{A} \kappa^{2}}{(\sqrt{a/b} + \sqrt{b/a})\pi^{2}} \sum_{n,m=0}^{\infty} \left(A\kappa^{2} + (2n+1)^{2} \frac{\pi^{2}b}{a} + (2m+1)^{2} \frac{a\pi^{2}}{b} \right)^{-1}.$$
(44)

and the integral capacitance per unit length of the rectangular pore is

 $\left(\frac{b}{(2m+1)^2a} + \frac{a}{(2n+1)^2b}\right)$

$$C_{I} = 4(a+b)C_{IL}$$

$$= \frac{64 \in_{0} \in_{r} A\kappa^{2}}{\pi^{2}} \sum_{n,m=0}^{\infty} \left(A\kappa^{2} + (2n+1)^{2} \frac{\pi^{2}b}{a} + (2m+1)^{2} \frac{a\pi^{2}}{b} \right)^{-1}.$$

$$\left(\frac{b}{(2m+1)^{2}a} + \frac{a}{(2n+1)^{2}b} \right)$$

$$(45)$$

Figure 3 shows the variation of the integral capacitance per unit length of the rectangular pore with the parameter of $\kappa \sqrt{A}$ for different aspect ratios of a/b. For comparison, the variation of the integral capacitance per unit length of a cylindrical pore with A in cross-sectional area for small electric potential (Eq. (43)) is also included in Fig. 3. It is evident that all the integral capacitances per unit length increase with

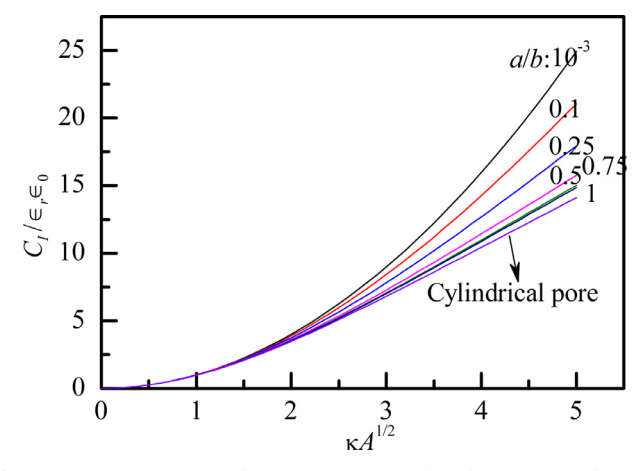


Figure 3. Variation of integral capacitance per unit length of a rectangular pore with cross-sectional area for different aspect ratios of a/b.

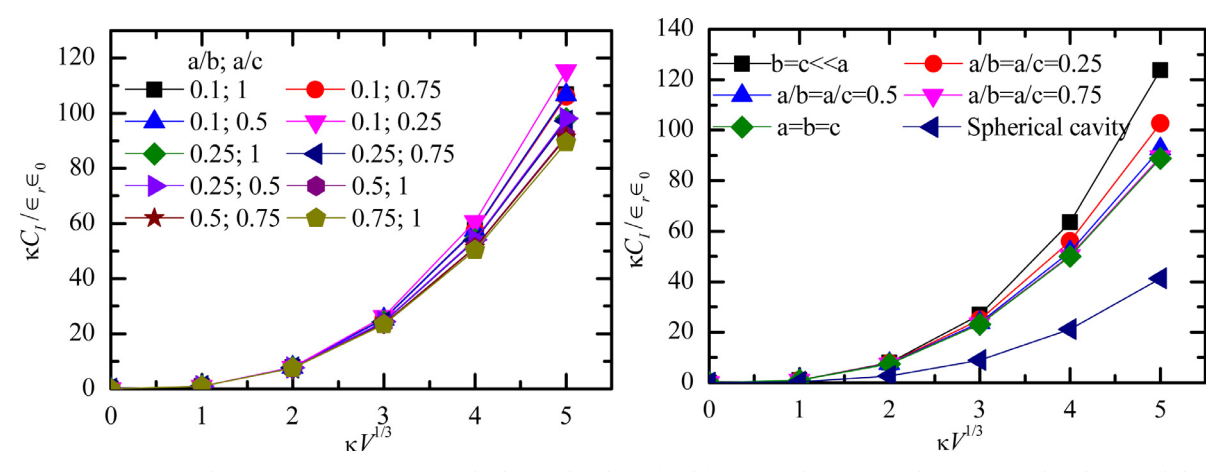


Figure 4. (a) Variation of integral capacitance of a 3D-rectangular box with volume for different combinations of the ratios of a/b and a/c, and (b) variation of integral capacitance of a 3D-rectangular box with volume for different ratios of a/b with b=c.

the increase of the cross-sectional area, as expected, which can be attributed to the increase of surface area with the increase of the crosssectional area. From Fig. 3, we note that the integral capacitance per unit length of the rectangular pore with the same cross-sectional area increases with the increase of the aspect ratio of a/b and is always larger than the cylindrical pore of the same cross-sectional area. Such behavior is due to that the cylindrical pore has the smallest surface area for the same cross-sectional area, and the surface area of a rectangular pore of a given cross-sectional area increases with the increase of the aspect ratio. Note a square pore, i.e. a=b, has the smallest integral capacitance among all the rectangular pores of the same cross-sectional area since $4(a+b) \ge 4A^{1/2}$ with the equality being held at a=b. These results suggest that rectangular pores of the same cross-section areas with large aspect ratios are preferred for the storage of ions, since more active sites are available for ions. That is to say, multi-layer structures, such as multilayer graphene, are preferred for supercapacitors. This trend can be illustrated as below from the calculation of the perimeters of a cylindrical pore and a rectangular pore of the same cross-section area, A.

The perimeter of a cylindrical pore, L_c , is

$$L_c = 2\sqrt{\pi A} \tag{46}$$

and the perimeter of a rectangular pore of $2a \times 2b$, L_r , is

$$L_r = \frac{A}{b} + 4b \ge 4\sqrt{A} > L_c = 2\sqrt{\pi A} \tag{47}$$

It is evident that increasing the aspect ratio of a/b increase the perimeter of the rectangular pore, leading to the increase of the active sites for the storage of ions.

Consider a cavity of V in volume. For a spherical cavity of V in volume under small electric potential, the integral capacitance per unit area is

$$C_{IL} = \in_r \in_0 \kappa \left(\coth[\kappa (3V/4\pi)^{1/3}] - \frac{1}{\kappa (3V/4\pi)^{1/3}} \right)$$
(48)

and the integral capacitance of the spherical cavity is

$$C_{I} = 4\pi r^{2} C_{IL} = 4\pi \in_{r} \in_{0} \kappa \left(\frac{3V}{4\pi}\right)^{2/3} \left(\coth\left[\kappa (3V/4\pi)^{1/3}\right] - \frac{1}{\kappa (3V/4\pi)^{1/3}} \right)$$
(49)

For a 3D rectangular box of V in volume, abc = V/8, Eq. (38) yields the integral capacitance per unit area as

$$C_{IL} = \frac{256 \in_{0} \in_{r} V^{1/3} \kappa^{2}}{\pi^{4}} \left[\left(\frac{bc}{a^{2}} \right)^{1/3} + \left(\frac{ac}{b^{2}} \right)^{1/3} + \left(\frac{ab}{c^{2}} \right)^{1/3} \right]^{-1}$$

$$\sum_{n,m,p=0}^{\infty} \frac{1}{(2n+1)^{2} (2m+1)^{2} (2p+1)^{2}} \cdot \left[V^{2/3} \kappa^{2} + (2n+1)^{2} \pi^{2} \left(\frac{bc}{a^{2}} \right)^{2/3} + (2m+1)^{2} \pi^{2} \left(\frac{ac}{b^{2}} \right)^{2/3} \cdot + (2p+1)^{2} \pi^{2} \left(\frac{ab}{c^{2}} \right)^{2/3} \right]^{-1}$$

$$\left[(2n+1)^{2} \left(\frac{bc}{a^{2}} \right)^{2/3} + (2m+1)^{2} \left(\frac{ac}{b^{2}} \right)^{2/3} + (2p+1)^{2} \left(\frac{ab}{c^{2}} \right)^{2/3} \right]$$

and the integral capacitance of the rectangular box is

$$C_{I} = 8(ab + bc + ac)C_{IL}$$

$$= \frac{512 \in_{0} \in_{r} V\kappa^{2}}{\pi^{4}} \sum_{n,m,p=0}^{\infty} \frac{1}{(2n+1)^{2}(2m+1)^{2}(2p+1)^{2}}.$$
(51)

$$\begin{split} & \left[V^{2/3} \kappa^2 + (2n+1)^2 \pi^2 \left(\frac{bc}{a^2} \right)^{2/3} + (2m+1)^2 \pi^2 \left(\frac{ac}{b^2} \right)^{2/3} \right. \\ & + (2p+1)^2 \pi^2 \left(\frac{ab}{c^2} \right)^{2/3} \right]^{-1} \end{split}$$

$$\left[(2n+1)^2 \left(\frac{bc}{a^2} \right)^{2/3} + (2m+1)^2 \left(\frac{ac}{b^2} \right)^{2/3} + (2p+1)^2 \left(\frac{ab}{c^2} \right)^{2/3} \right]$$

Figure 4a shows the variation of the integral capacitance of a 3D rectangular box with the volume of the cavity for different combinations of the ratios of a/b and a/c. It is evident that the all the integral capacitances increase with the increase of the cavity volume, as expected, which can be attributed to the increase of the surface area with the increase of the cavity volume. For the same cavity volume, the integral capacitance is dependent on the ratios of a/b and a/c. According to Fig. 4a, we note that decreasing the ratios of a/b and a/c leads to the increase of integral capacitance, i.e. the 3D rectangular cavity with the ratio of side length to width approaching zero is more efficient in the storage of ions for electrical-double layer capacitors. Note a cubic box, i.e. a=b=c, has the smallest integral capacitance since $8(ab+bc+ac) \ge 6V^{2/3}$ with the equality being held under a=b=c.

Figure 4b depicts the variation of the integral capacitance of a 3D rectangular box with the volume of the cavity for different ratios of a/b with b=c. For comparison, the variation of the integral capacitance of a

spherical cavity with V in volume for small electric potential (Eq. (49)) is also included in Fig. 4b. It is evident that the integral capacitance of the 3D rectangular box is always larger than the spherical cavity of the same volume. Such behavior is due to that the spherical cavity has the smallest surface area for the same cavity volume. Under the condition of b=c, the integral capacitance of the 3D rectangular box increases with the increase of the ratio of a/b i.e. the 3D rectangular box with a sheet-like cavity possesses the largest capacitance. Such a result suggests that sheet-like structures, such as multilayer graphene, are preferable for EDLCs in comparison to spherical cavity and cylindrical channels/pores. Note that the numerical result also reveals that the integral capacitance of the 3D rectangular box with b=c < a is the same as that with b=c>>a, suggesting again that the sheet-like structure is the preferable structure for the energy storage in EDLCs. This result is in accord with that the surface area of a 3D rectangular box increases with the increase of the aspect ratio of a/b (b=c) for the same volume and is larger than the surface of a spherical cavity of the same volume. Sheet-like structures possess more active sites available for the storage of ions.

Consider a cavity of V in volume. The surface area of a spherical cavity, S_s , is

$$S_{\rm s} = 4\pi \left(\frac{3}{4\pi}V\right)^{2/3} \tag{52}$$

and the surface area of a 3D rectangular box of $2a \times 2b \times 2c$, S_r , is

$$S_r = 8(ab + bc + ac) = V\left(\frac{1}{a} + \frac{1}{b} + \frac{1}{c}\right) \ge 6V^{2/3} > S_s = 4\pi \left(\frac{3}{4\pi}V\right)^{2/3}$$
(53)

It is evident that decreasing one of the dimensions of the 3D rectangular box can increase the active sites for the storage of ions.

Figure 5 shows the contour of the integral capacitance of a 3D-rectangular box with $\kappa V^{1/3} = 5$. It is evident that there is symmetric feature of the contour plot about the axis of b = c. Decreasing the ratio of a/b (a/c) under the same a/c (a/b) leads to the increase of the integral capacitance, and decreasing the ratios of a/b and a/c simultaneously can increase the integral capacitance relatively significantly.

5. Discussion

Practically, the materials used in EDLCs are porous materials, which are characterized normally by porosity and tortuosity. The other

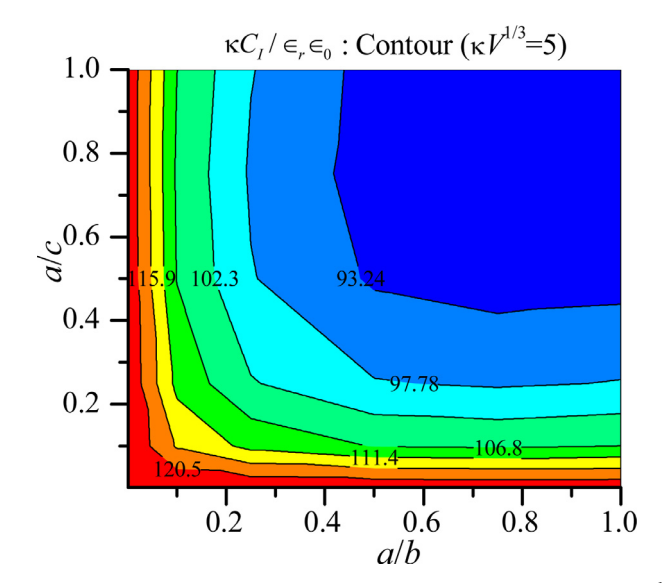


Figure 5. Contour plot of integral capacitance of a 3D-rectangular box for $\kappa V^{1/3} = 5$

important parameters widely used to determine the electrochemical performance of the "active" materials used in EDLCs are the surface area and the fractions of micropores (<2 nm), mesopores (2-50 nm) and macropores (>50 nm). In general, both the porosity and the surface area likely co-determine the energy storage in EDLCs, and there exists correlation between the porosity and the surface area.

For simplicity, we consider a porous material consisting of parallel, straight pores of through thickness. The porosity of the porous material, ϕ , is

$$\phi = \frac{V_V}{V_T} = \frac{S_C}{S_T} \tag{54}$$

where V_T and S_V are the resultant volume and cross-sectional area of pore space, respectively, and V_T and S_C are the total volume and cross-sectional area of the porous material, including the solid and pore spaces. Assume that all the parallel, straight pores have the same cross section and the number of the parallel, straight pores is χ . Using Eq. (54), we obtain the cross-sectional area, S_p , of a straight pore as

$$S_p = \frac{S_T \phi}{\chi} \tag{55}$$

In the following, we consider two simple geometric configurations of the parallel, straight pores; the first one is cylindrical pores of r in radius, and the second one is square-like pores with 2a in the side length.

For the cylindrical pores of r in radius, the radius, r, is found from Eq. (55) as

$$r = \left(\frac{S_T \phi}{\pi \chi}\right)^{1/2} \tag{56}$$

which gives the total surface area for the parallel, cylindrical pores, S_T , as

$$S_T = 2\pi r \chi L = 2L(\pi \chi S_T \phi)^{1/2}$$
(57)

Here, L is the length of the parallel, cylindrical pores (the depth of the porous material). Using Eq. (43), we obtain the integral capacitance of the porous material, C_{TC} , which consists of parallel, cylindrical pores of r in radius, as

$$C_{TC} = 2 \in_{r} \in_{0} \kappa L(\pi \chi S_{T} \phi)^{1/2} I_{1} \left[\kappa \left(\frac{S_{T} \phi}{\pi \chi} \right)^{1/2} \right] \left(I_{0} \left[\kappa \left(\frac{S_{T} \phi}{\pi \chi} \right)^{1/2} \right] \right)^{-1}$$
(58)

For the square-like pores of 2a in side length, the side length, 2a, is found from Eq. (55) as

$$2a = \left(\frac{S_T \phi}{\chi}\right)^{1/2} \tag{59}$$

which gives the total surface area for the parallel, square-like pores, S_T , as

$$S_T = 4L(\chi S_T \phi)^{1/2} \tag{60}$$

Using Eq. (27), we obtain the integral capacitance of the porous material, C_{TS} , which consists of parallel, square-like pores of 2a in side length, as

$$C_{TS} = \frac{64 \in_{0} \in_{r} L\chi\kappa^{2}}{\pi^{2}} \sum_{n,m=0}^{\infty} \frac{1}{(\kappa^{2} + \lambda_{nm}^{2})} \left(\frac{1}{(2m+1)^{2}} + \frac{1}{(2n+1)^{2}} \right)$$
 (61)

with the eigenvalues, λ_{nm} , as

$$\lambda_{nm}^{2} = 4\pi^{2} \left[\left(n + \frac{1}{2} \right)^{2} + \left(m + \frac{1}{2} \right)^{2} \right] \left(\frac{S_{T} \phi}{\chi} \right)^{-1}$$
(62)

According to Eqs. (58) and (61), we can conclude that the integral capacitance of a porous material is dependent on the porosity, the cross-sectional area and the number of pores, which determine the total surface area (active sites) available for the energy storage. It needs to be

pointed out that the results presented in Eqs. (58) and (61) represent the maximum capacitance achievable by a porous material for the cylindrical and square-like pores, respectively, in which all the pores possess the same cross-sectional area. There are other factors, such as the migration rate of ions, likely determining the capacitance, which can be achieved during electrochemical cycling.

For porous materials with different pore structures, it is very difficult, if not impossible, to obtain analytical relations between the integral capacitance and the surface area (porosity and pore distribution) under small electric potential due to the dependence of the integral capacitance per unit area on the pore geometry, as revealed in Figs. 3 and 4. If the pore shape for a porous material possesses geometrical similarity, such as all pores being straight and cylindrical or square-like, the integral capacitance can be numerically calculated under the condition that the local distributions of the porosity and the pore density are known.

As an example, we consider a porous material with parallel, cylindrical pores. There are spatial distributions of both χ (the number of pores per unit area) and r (the pore radius). The integral capacitance can be calculated as

$$C_{TC} = 2\pi \in_{r} \in_{0} \kappa L \int_{\Xi} \frac{I_{1}(\kappa r)}{I_{0}(\kappa r)} r \chi d\Xi$$
(63)

with the integration over the cross section of the porous material.

6. Summary

In summary, we have brought out the importance of the geometric configurations of pore structures of porous materials in determining the capacity for the energy storage in electrical-double-layer capacitors under small electrical potential. Using the spectral method, we have solved the linearized Poisson-Boltzmann equation for three different geometrical shapes of the pores presented in porous materials, including slab-like structure, rectangular pore and 3d-rectangular box, and obtained analytical expressions of the integral capacitances of the three different geometrical shapes under small electric potential.

We have performed numerical calculation of the integral capacitances for the three different geometrical shapes. The numerical results for the slab-like are the same as those from the closed-form solution, validating the spectral method used in calculating the integral capacitances of porous materials under small electric potential. For the rectangular pore, the integral capacitance of the pore is always larger than the cylindrical pore with the same cross-sectional area. Increasing the aspect ratio of the rectangle-like pore increases the integral capacitance of the pore. For the 3D-rectangular box, the integral capacitance of the 3D-rectangular box is always larger than the spherical cavity with the same cavity volume. Increasing the aspect ratios of the 3D rectangular box increases the integral capacitance of the 3D rectangular box. It needs to be pointed out that the results obtained in this work also can be applied to the design of electrodes of mesosizes and microsizes, and are limited to the structures in which the effect of ionic size is negligible.

For porous materials with parallel, straight pores, we have developed analytical expressions for the integral capacitance as the functions of the porosity, the number of pores and the cross-sectional area for cylindrical and rectangular pores. A general method has been proposed to calculate the integral capacitance of a porous material if the pores are straight and the pore morphologies are similar.

CRediT author statement

WZ: Numerical calculation and Data curation; FY: Conceptualization, Methodology, Writing- Editing.

Declaration of Competing Interest

The authors declare that they have no known competing financial interests or personal relationships that could have appeared to influence the work reported in this paper.

Acknowledgement

FY is grateful for the support from the NSF, USA[CMMI-1634540], monitored by Dr. Khershed Cooper.

Supplementary materials

Supplementary material associated with this article can be found, in the online version, at doi:10.1016/j.est.2020.101477.

References

- J.R. Miller, P. Simon, Electrochemical capacitors for energy management, Science 321 (2008) 651–652.
- [2] G. Wang, L. Zhang, J. Zhang, A review of electrode materials for electrochemical supercapacitors, Chemical Society Reviews 41 (2012) 797–828.
- [3] R. Kötz, M. Carlen, Principles and applications of electrochemical capacitors, Electrochimica Acta 45 (2000) 2483–2498.
- [4] F. Yang, Size effect on electric-double-layer capacitances of conducting structures, Physics Letters A 383 (2019) 2353–2360.
- [5] W. Cao, F. Yang, Supercapacitors from high fructose corn syrup-derived activated carbons, Materials Today Energy 9 (2018) 406–415.
- [6] M.D. Stoller, R.S. Ruoff, Best practice methods for determining an electrode material's performance for ultracapacitors, Energy & Environmental Science 3 (2010) 1294–1301.
- [7] S. Cheng, L. Yang, Y. Liu, W. Lin, L. Huang, D. Chen, C. Wong, M. Liu, Carbon fiber paper supported hybrid nanonet/nanoflower nickel oxide electrodes for high-performance pseudo-capacitors, Journal of Materials Chemistry A 1 (2013) 7709–7716.
- [8] M.Z. Bazant, K. Thornton, A. Ajdari, Diffuse-charge dynamics in electrochemical systems, Physical Review E 70 (2004) 021506.
- [9] A.J. Bard, L.R. Faulkner, Electrochemical Methods: Fundamentals and applications, 2 nd edition, John. Wiley & Sons, Inc., New York, NY, 2000.
- [10] J.H. Masliyah, S. Bhattacharjee, Electrokinetic and colloid transport phenomena, John Wiley & Sons, Inc., New York, NY, 2006.
- [11] C.W. Outhwaite, L.B. Bhuiyan, An improved modified Poisson–Boltzmann equation in electric-double-layer theory, Journal of the Chemical Society, Faraday Transactions 2: Molecular and Chemical Physics 79 (1983) 707–718.
- [12] V. Vlachy, Ionic effects beyond Poisson-Boltzmann theory, Annual Review of Physical Chemistry 50 (1999) 145–165.
- [13] J. Bikerman, Structure and capacity of electrical double layer, The London, Edinburgh, and Dublin Philosophical Magazine and Journal of Science 33 (1942) 384–397.
- [14] S.W. Kenkel, J.R. Macdonald, A lattice model for the electrical double layer using finite-length dipoles, The Journal of Chemical Physics 81 (1984) 3215–3221.
- [15] A.A. Kornyshev, The simplest model of charge storage in single file metallic nanopores. Faraday Discussions 164 (2013) 117–133.
- [16] K. Johannessen, The exact solution to the one-dimensional Poisson–Boltzmann equation with asymmetric boundary conditions, Journal of Mathematical Chemistry 52 (2014) 504–507.
- [17] J.P. Hsu, M.T. Tseng, Solution to linearized Poisson–Boltzmann equation with mixed boundary condition, The Journal of chemical physics 104 (1996) 242–247.
- [18] H. Saboorian-Jooybari, Z. Chen, Analytical solutions of the Poisson-Boltzmann equation within an interstitial electrical double layer in various geometries, Chemical Physics 522 (2019) 147–162.
- [19] H. Ohshima, T.W. Healy, Accurate analytic expressions for the surface charge density/surface potential relationship and double-layer potential distribution for a spherical colloidal particle, Journal of Colloid and Interface Science 90 (1982) 17–26.
- [20] H.-K. Tsao, Counterion distribution enclosed in a cylinder and a sphere, The Journal of Physical Chemistry B 102 (1998) 10243–10247.
- [21] D.A. Iozzo, M. Tong, G. Wu, E.P. Furlani, Numerical analysis of electric double layer capacitors with mesoporous electrodes: Effects of electrode and electrolyte properties, The Journal of Physical Chemistry C 119 (2015) 25235–25242.
- [22] E.J. Dickinson, R.G. Compton, Diffuse double layer at nanoelectrodes, The Journal of Physical Chemistry C 113 (2009) 17585–17589.
- [23] M.S. Uddin, H.T. Das, T. Maiyalagan, P. Elumalai, Influence of designed electrode surfaces on double layer capacitance in aqueous electrolyte: Insights from standard models, Applied Surface Science 449 (2018) 445–453.
- [24] M. Feit, J. Fleck Jr, A. Steiger, Solution of the Schrödinger equation by a spectral method, Journal of Computational Physics 47 (1982) 412–433.